Quaternary Science Reviews 72 (2013) 137–145

Contents lists available at SciVerse ScienceDirect

Quaternary Science Reviews

journal homepage: www.elsevier.com/locate/quascirev

Quantitative temperature reconstruction based on growth rate of annually-layered stalagmite: a case study from central China

Liangcheng Tan [a,*], Liang Yi [b], Yanjun Cai [a], Chuan-Chou Shen [c], Hai Cheng [d,e], Zhisheng An [a]

[a] State Key Laboratory of Loess and Quaternary Geology, Institute of Earth Environment, Chinese Academy of Sciences, Xi'an 710075, China
[b] State Key Laboratory of Lithospheric Evolution, Institute of Geology and Geophysics, Chinese Academy of Sciences, Beijing 100029, China
[c] High-precision Mass Spectrometry and Environment Change Laboratory (HISPEC), Department of Geosciences, National Taiwan University, Taipei 106, Taiwan
[d] Institute of Global Environmental Change, Xi'an Jiaotong University, Xi'an 710049, China
[e] Department of Earth Sciences, University of Minnesota, Minneapolis 55455, USA

ARTICLE INFO

Article history:
Received 1 May 2012
Received in revised form
26 April 2013
Accepted 29 April 2013
Available online

Keywords:
Stalagmite
Annual layer
Growth rate
Temperature
Modern process
Central China

ABSTRACT

We used the annual growth rate of a stalagmite (XL21) collected from Xianglong Cave, central China, to quantitatively reconstruct regional terrestrial temperature changes over the last 95 years (1912–2006 AD). Based on a significant positive correlation between the growth rate and the observed temperature, a transfer function was designed, and the temperature from the previous September to May (P_9-5) was reconstructed, with an explained variance of 43.5%. Our results show an increasing trend in temperature during the last century, and especially over the last 30 years. The temperature variability from central China recorded here bears a striking similarity to that in the Northern Hemisphere, and also to global trends. However, the cooling between the 1980s and the early 1990s seen in the stalagmite record, which interrupted the warming trend that began in the 1960s, is not observed in the mean conditions found in China, the Northern Hemisphere, neither globally. This methodology for reconstructing historical temperature from stalagmite growth rates overcomes the limitation of the short meteorological observation period and supports the potential of stalagmite lamina climatology.

1. Introduction

The rapid warming trend of recent decades has been identified from meteorological observations (IPCC, 2007). The average temperature in China increased by 1.1 °C over the last 50 years (Ding et al., 2007), which is much larger than the global average increase (0.65 °C; IPCC, 2007). A better understanding of past temperature trends and the mechanisms, that drive this variability, is necessary if we are to improve the predictions made by climate models. Limited modern instrumental observations, however, hinder our understanding of regional and global climate changes. Therefore, it is important to obtain robust high-resolution proxy records to extend the period currently covered by the relatively short-term instrumental temperature records.

Most of the high-resolution proxy-inferred temperature records from mainland China are based on tree ring data (e.g., Liu et al., 2005, 2009a,b; Gou et al., 2008; Li et al., 2012; Shao, 2012; Chen et al., 2013; Zhang et al., 2013), although some are derived from historical documents (Ge et al., 2003, 2010; Yang, 2007; Chu et al., 2012; Hao et al., 2012) or ice cores (Yao et al., 1997, 2006; Wang et al., 2003, 2006; Thompson et al., 2006; Yang et al., 2009). Comparison between multi-proxy records can reduce the uncertainties associated with single proxy reconstructions (Tan et al., 2011). Annual laminae from speleothems can be used to develop high-resolution paleoclimatic or palaeoenvironmental records through the correlation of lamina thickness (annual growth rate) with climate parameters such as rainfall (Brook et al., 1999; Proctor et al., 2000; Burns et al., 2002; Baker et al., 2007) and temperature (Frisia et al., 2003; Tan et al., 2003). For example, a temperature reconstruction spanning 2650 years was derived from the varying thickness of annual layers preserved in a stalagmite from Shihua Cave, northern China (Tan et al., 2003). Tan et al. (2006) summarized their climatic applications and suggested that laminated stalagmites, as well as tree rings, can provide complementary climatic information.

In this study, we apply the dendroclimatological method to stalagmite lamina climatology (Tan et al., 2006), and quantitatively reconstruct a temperature record for the last 95 years (1912–2006

* Corresponding author. Tel.: +86 29 88323194.
E-mail addresses: tanlch@ieecas.cn, tlch1209@163.com (L. Tan).

0277-3791/$ – see front matter © 2013 Elsevier Ltd. All rights reserved.
http://dx.doi.org/10.1016/j.quascirev.2013.04.022

AD) using the growth rate of an annually-layered stalagmite from Xianglong Cave, which is located on the southern flank of the Qinling Mountains, central China. With the exception of a period of cooling during the 1980s and early 1990s, the pattern of temperature change in central China over the last 95 years is similar to that in the Northern Hemisphere and at a global scale.

2. Cave location and sample description

Qinling Mountains are the watershed of the Yangtze and Yellow rivers, and also a key climatic boundary in China. Regional climate to the north of the Qinling Mountains is temperate sub-humid, but to the south it is subtropical humid (Zhao, 1995). It has been suggested that there are regional differences in rainfall variations over the last 750 years between the central and western Qinling Mountains (Tan et al., 2009). Meanwhile, temperature variations reconstructed from tree ring data show broad similarities across the Qinling Mountains (Liu et al., 2009b).

Located on the southern flank of the Qinling Mountains, Xianglong Cave (33°00′N, 106°20′E, 940 m above sea level (asl) at the entrance) is more than 1.2 km in length, with several branched passages and many chambers (Fig. 1). The humidity of the inner channels is around 100%. Drip rates of cave water range from 2 to 99 drops per minute, and recharge to the karst aquifer above the cave is thought to be derived from meteoric precipitation. Instrumental climate data from the nearest meteorological station, Ningqiang station (20 km southwest of Xianglong Cave), indicate a mean annual air temperature of 13 °C, and a mean annual rainfall of 1100 mm. Most of the rainfall (>70%) occurs during the summer monsoon months (June–October; Liu et al., 2003). We calculated the water balance at the cave site using the Thornthwaite evapotranspiration model (Thornthwaite, 1948; McCabe and Markstrom, 2007). As shown in Fig. 2, most of the water surplus occurs between July and October. Consequently, recharge of the aquifer in this area occurs mainly from summer monsoon rainfall. Vegetation is abundant above the cave with evergreen broad leaf forest.

An active stalagmite (XL21; Fig. 3), 4.2 cm in length and receiving drip water from the ceiling, was collected about 700 m from the entrance of the cave in October 2009. The halved and polished stalagmite section shows clear laminae with alternations from a dark, compacted layer (DCL) to a white, porous layer (WPL). The uppermost 3.1 cm is composed of pure aragonite, but the lithology changed to calcite below 3.1 cm. Only the upper 2.9 cm segment was used in this study.

3. Methods

Subsamples of the stalagmite were obtained for ^{230}Th dating by drilling along the growth axis with a hand-held carbide dental drill. The chemical procedures used to separate uranium and thorium followed those described in Edwards et al. (1987) and Shen et al. (2003). Measurement of uranium and thorium was performed on a multi-collector inductively coupled plasma mass spectrometer (MC-ICPMS, Thermo-Finnigan Neptune) at the Minnesota Isotope Laboratory, USA (Cheng et al., 2009; Shen et al., 2012). Corrections for initial ^{230}Th were made assuming an initial ^{230}Th/^{232}Th atomic ratio of $4.4 \pm 2.2 \times 10^{-6}$. Lamina counting was also carried out on the visible laminae observed in the polished surface of the stalagmite.

The development of micromilling techniques has improved the spatial resolution of sampling, and it may now be possible to obtain the annual cycle of δ^{18}O variability preserved in a speleothem, offering an accurate chronology based on cycle counting (McDermott, 2004). Here, we performed stable isotope analysis

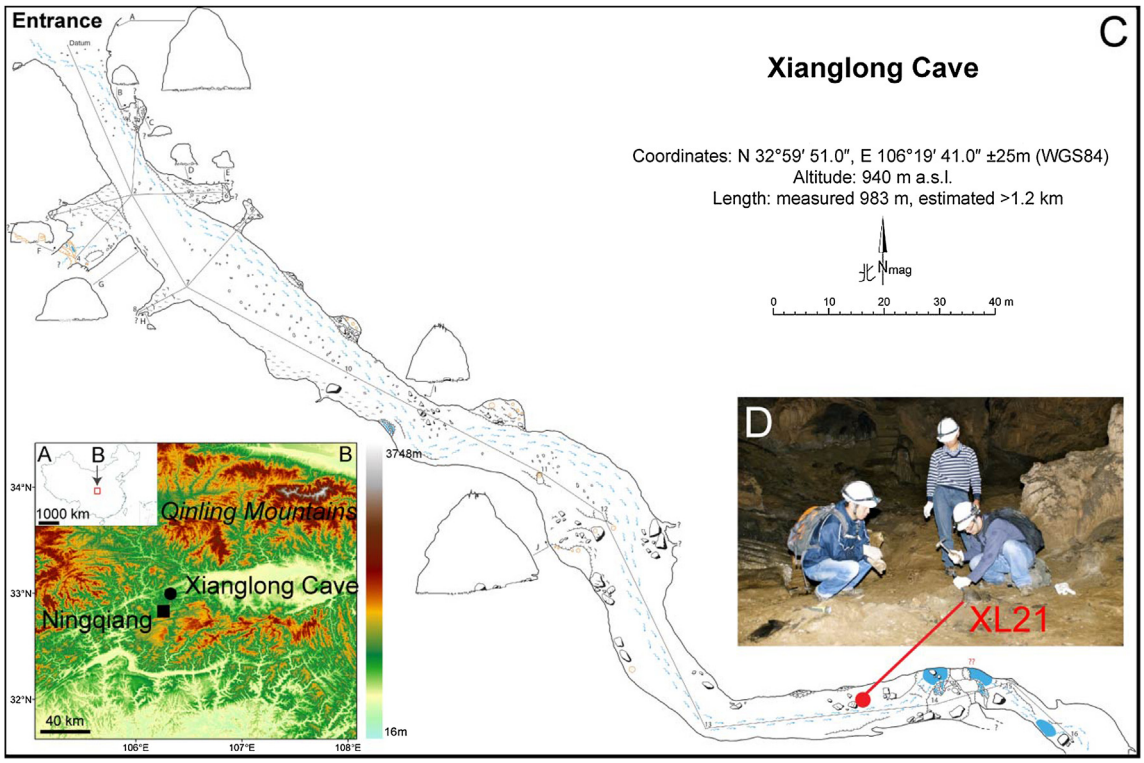

Fig. 1. Location and plan view of Xianglong Cave. (A) Overview map showing the study region. (B) Enlarged regional topographic map showing the location of Xianglong Cave. The Ningqiang station and the Qinling Mountains are also shown. Topographic GTOPO30 data from the USGS EROS Center (Earth Resources Observation and Science Center: http://eros.usgs.gov/#/Find_Data/Products_and_Data_Available/gtopo30_info). (C) Plan view of Xianglong Cave. (D) Photograph showing the sampling site of stalagmite XL21 in the cave.

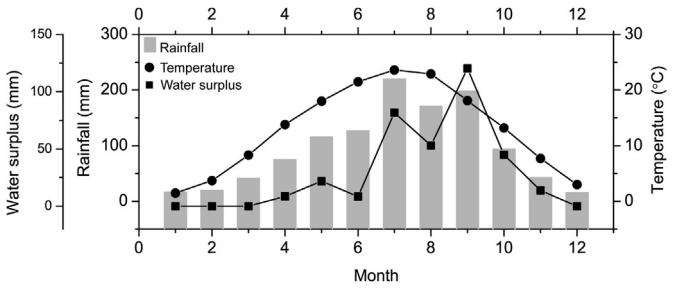

Fig. 2. Monthly rainfall (gray bars), temperature (circles), and water surplus (squares) at Ningqiang station (data: from 1957 to 2009 AD). The mean annual rainfall and temperature were 1100 mm and 13 °C, respectively, at this site. Most of the water surplus occurs between July and October.

($\delta^{18}O$ and $\delta^{13}C$) at intervals of 50 μm, using a New Wave Research Micromill, and analyzed the samples with an on-line, automated carbonate preparation system (Kiel III) linked to a Finnigan MAT-252 gas source mass spectrometer at the Institute of Earth Environment, Chinese Academy of Sciences. International standard NBS19 and inter-laboratory standard TTB1 were run every 10 to 15 samples, and arbitrarily selected duplicates were run every 15 to 20 samples to check for homogeneity and reproducibility. The $\delta^{18}O$ values reported here are expressed relative to the Vienna PeeDee Belemnite (VPDB) standard. The standard results show that the precision of the $\delta^{18}O$ analysis was better than 0.1‰ (2σ).

4. Results and discussion

4.1. Chronology and growth rate

U–Th isotopic compositions are listed in Table 1. An average $^{230}Th/^{232}Th$ atomic ratio of $4.4 \pm 2.2 \times 10^{-6}$, was used to calculate corrected ^{230}Th dates. This initial $^{230}Th/^{232}Th$ ratio is estimated for a material at U-series isotopic secular equilibrium with the crustal Th/U value of 3.8 (Taylor and McLennan, 1995) and arbitrary variability of 50%. The corrected ^{230}Th date of 2012 ± 9 AD for the upmost subsample, XL21-1A, is in agreement with the sampling time of the stalagmite (October 2009 AD), indicating that the stalagmite was actively growing when sampled. The agreement also indicates that the initial $^{230}Th/^{232}Th$ ratio is well evaluated.

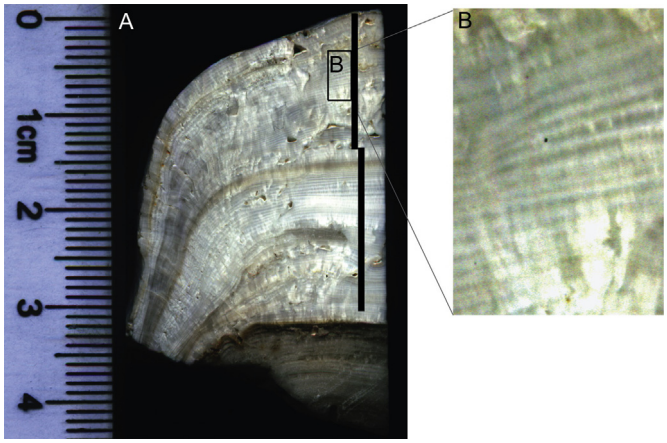

Fig. 3. (A) Section of stalagmite XL21 with micromilling paths (thick black lines) for C/O isotopic analysis. (B) Well-developed annual laminae with alternating dark compacted layers and white porous layers.

The determined four ^{230}Th dates (Table 1) show that the stalagmite deposited from 1914 ± 4 AD. A high-resolution $\delta^{18}O$ record, with 98 clear cycles, was recovered from the uppermost 2.9 cm of XL21. Agreement between $\delta^{18}O$ cycle counts, visible laminae counts, and ^{230}Th dates within analytical error, indicates that the DCL-WPL couplets and the $\delta^{18}O$ cycles are annual (Fig. 4). We used the counts of the $\delta^{18}O$ cycles to build the age–depth model and calculated the annual growth rate. The annual growth rate is equal to the sampling interval (50 μm) multiplied by the number of subsamples in every $\delta^{18}O$ cycle. It shows that the top 2.9 cm of the stalagmite grew from 1912 AD to the sampling time (October 2009 AD; Fig. 5). As the Micromill cannot accurately sample the boundaries of the annual layers, there may be some small errors ($<\pm 25$ μm) in the annual growth rate. These errors can be ignored when a timescale of several years is considered. We also optically measured the lamina thickness of the stalagmite for comparison. We calculated the average lamina thickness by measuring the thickness of every five laminae along the axis. As shown in Fig. 5, the annual growth rate calculated from the $\delta^{18}O$ cycles, with a higher resolution and accuracy, is coherent with the optically measured average lamina thickness. It shows that the growth rate of XL21 varied from 0.1 to 0.65 mm/yr, with an average of 0.3 mm/yr.

4.2. Climatic significance of stalagmite annual growth rate

Speleothem growth rates have a well-understood relationship with surface climate (e.g., Dreybrodt, 1980, 1981; Baker et al., 1998, 2007, 2008; Brook et al., 1999; Genty et al., 2001; Tan et al., 2003, 2006; Spötl et al., 2005; Fairchild et al., 2006; Baldini, 2010; Ruan and Hu, 2010; Cai et al., 2011; Duan et al., 2012; Mariethoz et al., 2012), primarily driven by the production of soil CO_2 due to changes in temperature and moisture (Dreybrodt, 1981; Baker et al., 1998, 2007; Tan et al., 2003, 2006). In semi-arid regions, stalagmite growth is moisture-limited (Polyak and Asmerom, 2001). As more water becomes available, the drip rate may increase and prolong deposition during the dry season (Brook et al., 1999). Therefore, growth rates can act as a reliable indicator of variations in rainfall amounts (Brook et al., 1999; Polyak and Asmerom, 2001; Vaks et al., 2003; Baker et al., 2007). The situation is more complex in humid and semi-humid regions because other factors, such as drip rate, atmospheric P_{CO_2} in the cave, and the seasonality of the surface climate may also affect speleothem growth rates (Baker et al., 1998; Fairchild et al., 2006; Baldini, 2010; Cai et al., 2011; Duan et al., 2012). For example, in a study in Scotland the speleothem layer thickness was found to be negatively correlated with annual mean rainfall (Proctor et al., 2000). In contrast, a study in northern Italy showed a significant positive correlation between the stalagmite annual growth rate and winter temperature (Frisia et al., 2003). Tan et al. (2003) suggested that, with an adequate water supply, the growth rate of a stalagmite from Shihua Cave in northern China was controlled by warm-season temperature variability.

We compared the annual growth rate series from XL21 with the temperature and rainfall records from the Ningqiang meteorological station (1957–2009 AD) to ascertain the precise climatic significance of its changing growth rate. Correlation analysis showed that the growth rate of XL21 is closely related to temperature variability, but not rainfall (Table 2). Due to the possible soil CO_2 and seepage water reservoir in the epikarst zone (Bar-Matthews et al., 1996; Frisia et al., 2003; Fairchild et al., 2006; Tan et al., 2006; Baker and Bradley, 2010), a smoothing and lag effect may exist in the response of the growth rate to climatic changes. Considering the autocorrelation in the temperature series (Kalvová and Nemesová, 1998; Xiao et al., 2010), a three-point

Table 1
U–Th isotopic data and ^{230}Th dates of stalagmite XL21.

Sample number	Depth from top (cm)	^{238}U (ppb)	^{232}Th (ppt)	^{230}Th/^{232}Th (atomic × 10^{-6})	δ^{234}U (measured)	^{230}Th/^{238}U (activity)	^{230}Th age (yr) (uncorrected)	^{230}Th age (yr BP) (corrected)	$\delta^{234}U_{Initial}$ (corrected)	^{230}Th age (yr AD) (corrected)
XL21-1A	0.1	4685.2 ± 19.5	4057.0 ± 12.7	3.5 ± 0.2	324.6 ± 4.2	0.00018 ± 0.00001	15 ± 1	−62 ± 9	324.6 ± 4.2	2012 ± 9
XL21-1	0.7	3601.0 ± 13.1	807.3 ± 16.4	24.9 ± 1.2	323.9 ± 3.7	0.00034 ± 0.00001	28 ± 1	−37 ± 4	323.9 ± 3.7	1987 ± 4
XL21-2	2.35	4507.1 ± 17.7	2517.7 ± 51.3	30.1 ± 0.8	317.4 ± 4.1	0.00102 ± 0.00002	84 ± 2	12 ± 9	317.4 ± 4.1	1938 ± 9
XL21-3	2.9	4925.6 ± 13.2	1168.8 ± 23.6	84.9 ± 2.1	322.4 ± 2.7	0.00122 ± 0.00002	101 ± 1	36 ± 4	322.5 ± 2.7	1914 ± 4

Note: Analytical errors are 2s of the mean. Decay constant values are: $\lambda_{230} = 9.1705 \times 10^{-6}\,y^{-1}$, $\lambda_{234} = 2.82206 \times 10^{-6}\,y^{-1}$ (Cheng et al., 2009) and $\lambda_{238} = 1.55125 \times 10^{-10}\,y^{-1}$ (Jaffey et al., 1971). Depths along the growth axes are relative to the top (youngest surface) of the stalagmite.

weighted averaging of the temperature record was developed as follows:

$$temp_1 = \frac{T_1 + T_2}{2}, \ldots, temp_i = \frac{T_{i-1} + T_{i+1}}{2}, temp_n = \frac{T_{n-1} + T_n}{2} \quad (1)$$

where $temp_i$ is the average temperature and T_i is the original temperature. The subscript 1 represents the initial year, and n represents the final year. Applying this moving-average smoothing generated the highest correlation coefficient ($r = 0.53$, $p < 0.01$; Table 2) between the annual growth rate and temperature from the previous September to the current May (P_9-5).

The correlation analysis suggests that temperature is the primary factor controlling growth rate variability in XL21 via its influence on the production of CO_2 in the soil overlying the cave (Baker et al., 1998; Tan et al., 2003, 2006). In summer, plentiful monsoon rainfall in this area may disturb the relationship between the growth rate and temperature (Table 2) by affecting the cave's drip rate and aragonite supersaturation, and thereby aragonite precipitation (Baker et al., 1998; Burns et al., 2002; Mattey et al., 2008; Duan et al., 2012). As a result, variability in the annual growth rate of XL21 reflects the temperature variability of P_9-5 ($r = 0.53$, $p < 0.01$) better than it does the annual mean temperature ($r = 0.45$, $p < 0.05$).

4.3. Temperature reconstruction over the last hundred years

Based on the correlation analysis between the growth rate of XL21 and the instrumental temperature record, a linear regression technique based on the bootstrap resampling method (Cook, 1990) was used to reconstruct the temperature of P_9-5. The modeling period was 1957–2008 AD. Two transfer functions were developed as follows.

(1) One-variable linear regression with no lag effect (1912–2008 AD):

$$temp = 9.26 + 1.46 \times growth\ rate \quad (2)$$

The explained variance R^2 was 27.8%, and the adjusted explained variance R^2_{adj} was 26.4%, with an F value of 19.25. All of the parameters were significant at $p < 0.01$.

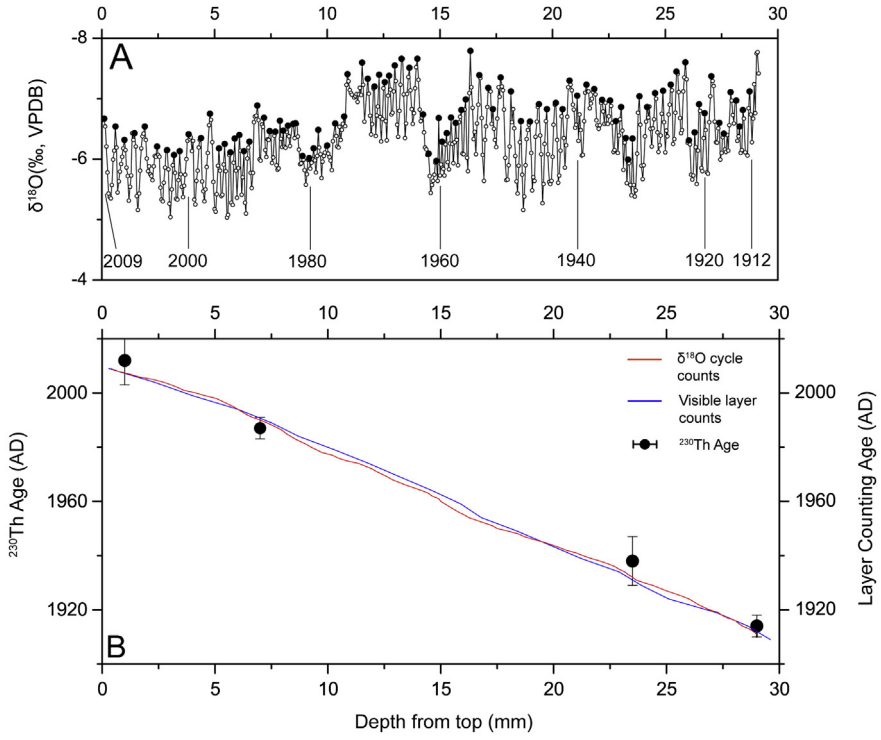

Fig. 4. (A) High-resolution intra-annual $\delta^{18}O$ time series of stalagmite XL21. (B) Comparison of age models based on visible annual layers (blue line), annual $\delta^{18}O$ cycles (red line), and ^{230}Th dates (solid circles). (For interpretation of the references to color in this figure legend, the reader is referred to the web version of this article.)

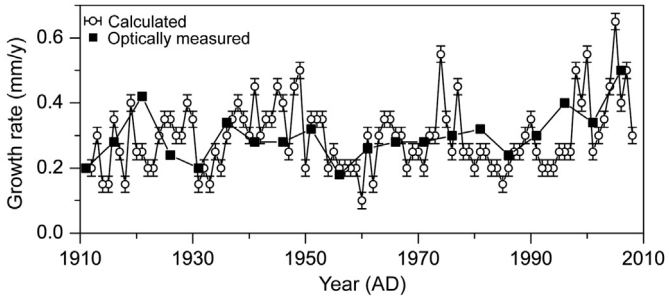

Fig. 5. Comparison annual growth rate series inferred from $\delta^{18}O$ record (hollow circles) and optical measurement of lamina thicknesses. Based on the $\delta^{18}O$ record, the growth rate of XL21 varies from 0.1 to 0.65 mm/yr, with an average of 0.3 mm/yr.

Considering the smoothing and lag effect, as well as a significant cross-correlation coefficient ($r = 0.56$, $p < 0.01$) between the growth rate and the *temp* series with a two-year lag, we developed a second transfer function as follows.

(2) Two-variable linear regression with a two-year lag (1912–2006 AD):

$$temp = 9.05 + 0.94 \times growth\ rate + 1.2 \times growth\ rate_{2yr-lag} \quad (3)$$

The $growth\ rate_{2yr\text{-}lag}$ represents the growth rate series with a two-year lag. The explained variance R^2 was 43.5%, and the adjusted explained variance R^2_{adj} was 41.1%, with an F value of 18.08. All of the parameters were significant at $p < 0.01$.

As shown in Fig. 6, the two reconstructed records and the instrumental temperature record are consistent. To further assess the statistical fidelity of the two reconstructions, we employed a split-sample calibration–verification process (Meko and Graybill, 1995). First, as in Cook et al. (1999), we split the samples into two groups: a calibration group and a verification group. Then, we evaluated the fidelity of the various climate reconstructions using standard measures of cross-validation reconstructive skill (e.g., Cook et al., 1999, 2010; Yi et al., 2012). The statistical parameters

Table 2
Correlation-coefficient matrix between stalagmite annual growth rate and meteorological records from Ningqiang station over the period 1957–2008 AD. *temp* represents the three-point weighted average temperature.

Month	Precipitation	Temperature	*temp*
P_9	0.25	0.04	0.26
P_{10}	0.13	0.23	0.20
P_{11}	−0.23	0.04	0.01
P_{12}	0.02	−0.28	−0.10
1	0	−0.02	**0.34***
2	0.02	0	**0.33***
3	−0.02	0.15	0.31
4	0.14	**0.44***	0.24
5	0	0.11	0.15
6	−0.14	0.06	0.12
7	−0.04	−0.02	0.09
8	−0.12	−0.04	−0.13
9	0.17	**0.39***	0.19
Winter (DJF)	0.02	−0.13	**0.33***
Spring (MAM)	0.07	**0.40***	**0.42***
Summer (JJA)	−0.13	0	0.03
Autumn(SON)	0.15	**0.33***	0.31
Annual (J-D)	0	0.27	**0.45***
P_9-5	–	0.23	**0.53****

Note: * and ** indicate significance levels of 95% and 99%, respectively. The sample size N is 52 (1957–2008 AD).

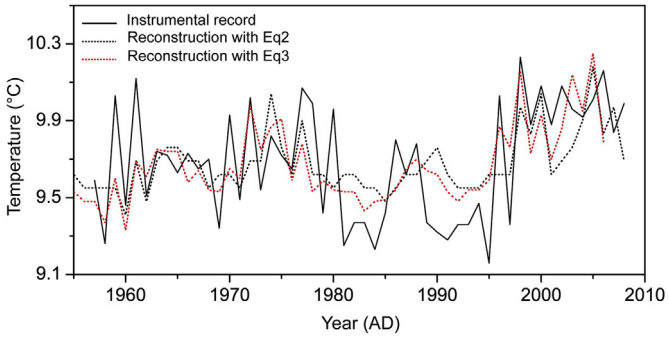

Fig. 6. Comparison between observed (black line) and reconstructed temperature records using Eq. (2) (dotted black line) and Eq. (3) (dotted red line). (For interpretation of the references to color in this figure legend, the reader is referred to the web version of this article.)

included the explained variance ($r(v)^2$), the Reduction of Error (RE), and the Coefficient of Efficiency (CE):

$$r(v)^2 = \frac{\left[\sum (X_i - \overline{X}_v)\left(\widehat{X}_i - \overline{\widehat{X}}_v\right)\right]^2}{\sum (X_i - \overline{X}_v)^2 \sum \left(\widehat{X}_i - \overline{\widehat{X}}_v\right)^2}, RE = 1 - \frac{\sum \left(X_i - \widehat{X}_i\right)^2}{\sum (X_i - \overline{X}_c)^2},$$

$$CE = 1 - \frac{\sum \left(X_i - \widehat{X}_i\right)^2}{\sum (X_i - \overline{X}_v)^2}$$

where X_i and $\widehat{X}_i$ are the observed and estimated data in year i of the verification period. $\overline{X}_v$ and $\overline{\widehat{X}}_v$ are the average values of the observed and estimated data during the verification period, and $\overline{X}_c$ is the average value of the observed data during the calibration period.

The following statements can be made regarding the method initially proposed by Cook et al. (1999).

(1) The value of $r(v)^2$ has a theoretical range between 0 and +1, and is the least rigorous of the three verification tests used here.
(2) The RE ranges from $-\infty$ to +1. An RE > 0 indicates reconstruction skill in excess of the climatology (i.e., $\overline{X}_c$), while an RE < 0 indicates less skill than the climatology.
(3) The CE is the most rigorous verification statistic of the three. CE has a theoretical range of $-\infty$ to +1. A CE > 0 indicates skill in excess of the verification period climatology (i.e., $\overline{X}_v$), while a CE < 0 indicates less skill than the verification period climatology (Cook et al., 1999).

According to the modeling period, the following two methods were used to split the dataset into calibration and verification subsets.

(1) The period 1957–1991 AD was set as the calibration period and 1992–2008 AD as the verification period. Then, the two periods were exchanged (1972–2008 AD was set as calibration data and 1957–1971 AD as verification data) (Cook et al., 1999).
(2) The dataset was divided into odd and even years to evaluate the models. Odd years were selected for the first calibration and verified with even years. For the second calibration, even years were used for calibration and odd years for verification (Linderholm and Chen, 2005; Yi et al., 2012). The results showed positive values of both RE and CE, which demonstrate the fidelity of these two transfer functions for temperature reconstruction (Table 3).

Table 3
Calibration–verification of the stalagmite-based *temp* transfer functions.

Statistics	Calibration (1957–1991)	Verification (1992–2008)	Calibration (1972–2008)	Verification (1957–1971)	Full calibration (1957–2008)	Statistics	Calibration (odd-year)	Verification (even-year)	Calibration (even-year)	Verification (odd-year)	Full calibration (all-year)
Eq. (2)						Eq. (2)					
r, $r(v)$	0.56	0.67	0.54	0.34	**0.53**	r, $r(v)$	0.32	0.54	0.58	0.56	**0.53**
R^2, $r(v)^2$	0.31	0.45	0.29	0.13	**0.28**	R^2, $r(v)^2$	0.1	0.29	0.33	0.31	**0.28**
RE	–	0.45	–	0.02	–	RE	–	0.21	–	0.27	–
CE	–	0.38	–	0.01	–	CE	–	0.05	–	0.11	–
Eq. (3)						Eq. (3)					
r, $r(v)$	0.61	0.72	0.76	0.58	**0.66**	r, $r(v)$	0.54	0.69	0.7	0.58	**0.66**
R^2, $r(v)^2$	0.38	0.52	0.57	0.33	**0.44**	R^2, $r(v)^2$	0.29	0.48	0.49	0.34	**0.44**
RE	–	0.6	–	0.09	–	RE	–	0.4	–	0.27	–
CE	–	0.55	–	0.08	–	CE	–	0.28	–	0.1	–

Note: r and $r(v)$ represent the Pearson correlation coefficient between the reconstructed and observed temperature series during calibration and verification period, respectively. R^2 and $r(v)^2$ represent the explained variance of the reconstructed temperature series during calibration and verification period, respectively.

The temperature record was reconstructed using these two transfer functions (Fig. 7). The quantitative reconstructions extend the instrumental temperature record back to 1912 AD. As the explained variance in Eq. (3) (43.5%) was greater than that in Eq. (2) (27.8%), we used the reconstruction from Eq. (3) to model the temperature variations of P_9-5 over the last 95 years in central China. The reconstructed temperature profile shows an increasing trend over the last 95 years, especially during the last 30 years. Four notably colder periods occurred: the early 1930s, the late 1950s, the early 1980s, and the early 1990s. Three notably warmer periods also occurred: from the late 1930s to the 1940s, the early 1970s, and from the late 1990s to the present.

4.4. Comparison with other records

Spatial correlation analysis between the temperature of P_9-5 at Ningqiang station and the CRU TS3.1 temperature gridded datasets (http://badc.nerc.ac.uk/view/badc.nerc.ac.uk__ATOM__dataent_1256223773328276) for the period 1958–2007 AD indicates that the temperature changed synchronously over central China during this period (Fig. 8). Therefore, our reconstruction can be used to represent regional temperature variability for central China. We compared our stalagmite-based temperature record with another winter half-year temperature reconstruction from the eastern Qinling Mountains based on tree ring data (Shi et al., 2009). The variability of the two series showed good agreement, especially at the decadal scale, confirming their reliability (Fig. 9). We also compared the stalagmite temperature record with the index of the East Asian winter monsoon (EAWM; Zhu, 2008). Although there is no significant correlation between the two series, the notable strengthening of the EAWM in the mid-late 1950s, the late 1960s, and the mid 1980s, corresponded well with the relatively cold intervals in central China (Fig. 9). This result suggests that the decreases in winter temperatures in central China may be related to the strengthening of the EAWM (Chen et al., 1999; Gong et al., 2001; Zhu, 2008).

Our temperature series shows close similarities to the winter half-year temperature variability over China ($r = 0.48$, $p < 0.01$; Tang et al., 2010), as well as temperature variability (P_9-5) over the Northern Hemisphere ($r = 0.39$, $p < 0.01$) and the global record ($r = 0.34$, $p < 0.01$) (Lawrimore et al., 2011; data source: GHCN-v3 1880-03/2012; Fig. 9). These findings indicate that temperature variability in central China follows a similar pattern to that in the Northern Hemisphere and the global record. The most notable regional characteristic of temperature variability in central China is

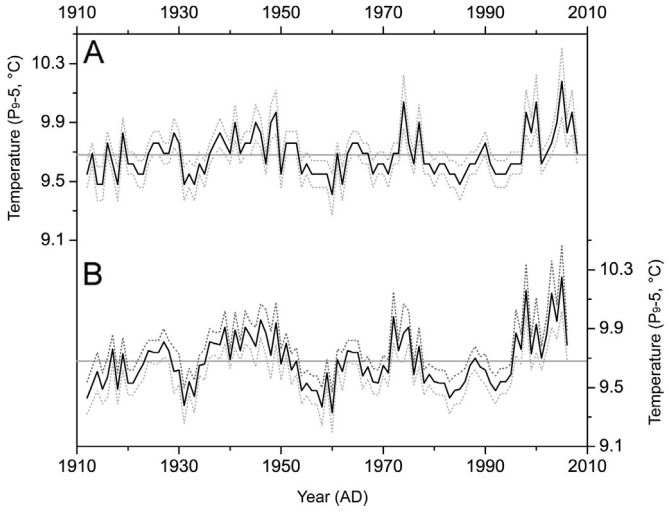

Fig. 7. Stalagmite-based temperature records for the previous September to May (P_9-5) over the last hundred years (black line) with 2σ error bar (dashed lines) using (A) one-variable linear regression with no lag effect, and (B) two-variable linear regression with a two-year lag. The gray lines represent the average temperature of 9.7 °C.

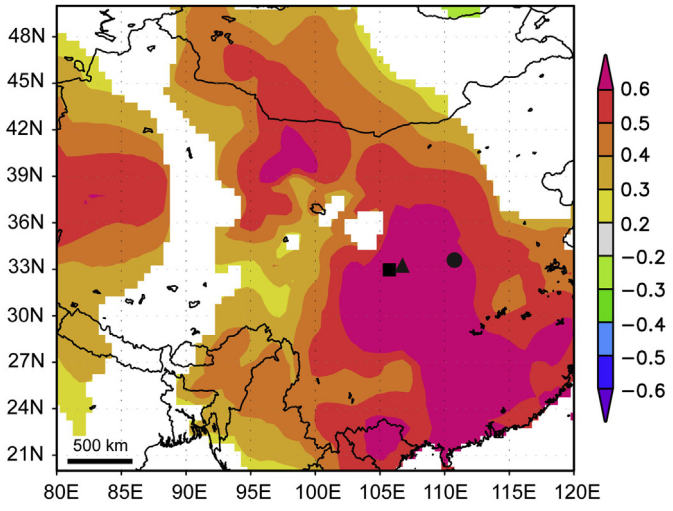

Fig. 8. Spatial correlation between P_9-5 temperature at Ningqiang station (square) and the CRU TS3.1 temperature grid datasets between 1958 and 2007 AD. Triangle and circle are locations of Xianglong Cave and the tree ring site in the Qinling Mountains, respectively. The scale on the right shows the correlation coefficients represented by different colors. (For interpretation of the references to color in this figure legend, the reader is referred to the web version of this article.)

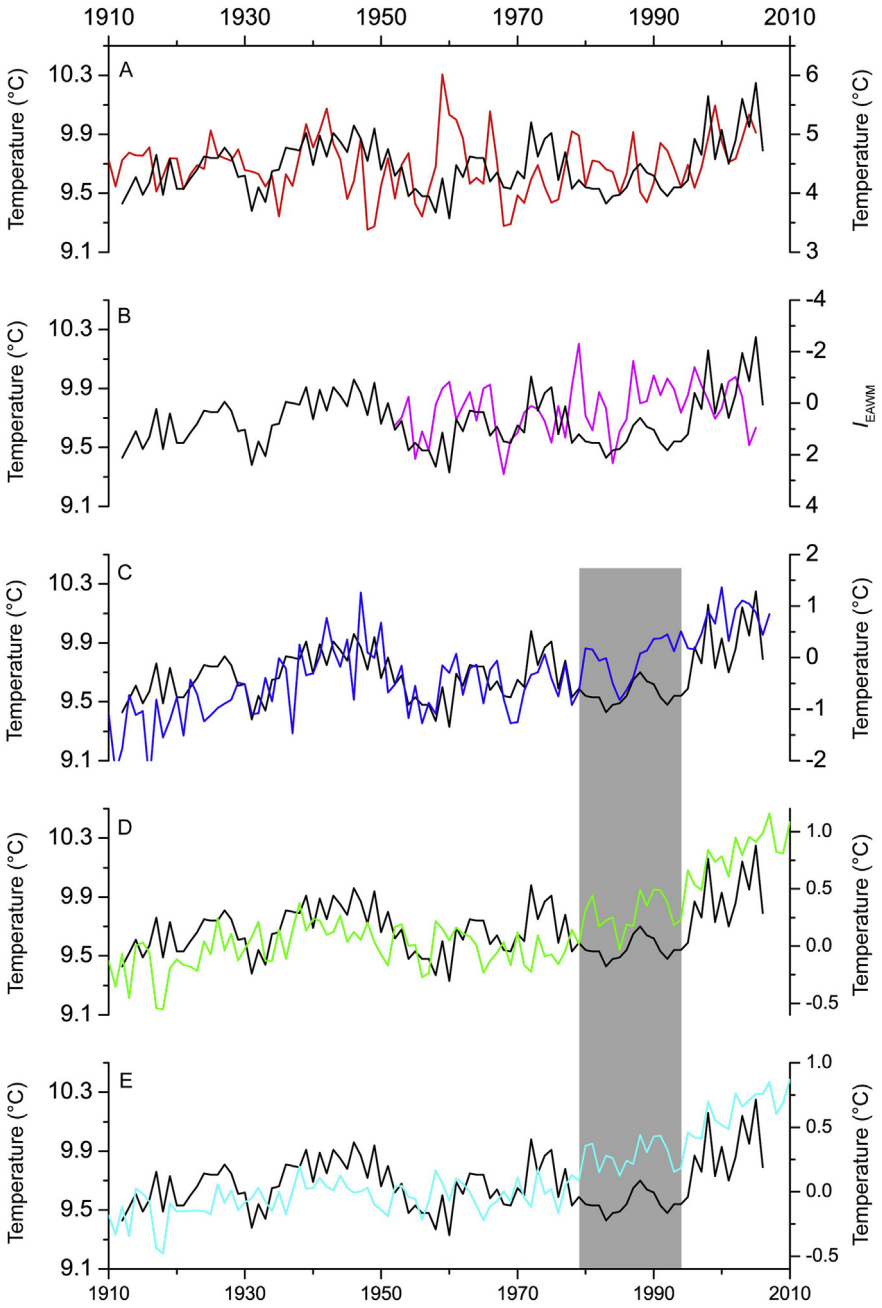

Fig. 9. Comparison of the stalagmite-based temperature reconstruction from this study (black lines) with other regional and global records: (A) temperature record based on tree ring data from the eastern Qinling Mountains (red) (Shi et al., 2009), (B) the East Asian winter monsoon (EAWM) index (purple) (Zhu, 2008), (C) the winter temperature in China (blue) (Tang et al., 2010), (D) P_9-5 temperature from the Northern Hemisphere (green) (Lawrimore et al., 2011; data from GHCN-v3 1880–03/2012), and (E) the global P_9-5 temperature (cyan) (Lawrimore et al., 2011; data from GHCN-v3 1880–03/2012). The gray bar indicates a cooling period between the 1980s and the early 1990s in central China, which is not evident in the mean series from China, the Northern Hemisphere, or the global record. (For interpretation of the references to color in this figure legend, the reader is referred to the web version of this article.)

the cooling between the 1980s and the early 1990s, which interrupted the warming trend that had persisted since the 1960s. This cooling is not recorded in either the national mean temperature series, or in the Northern Hemisphere or global means (Fig. 9), and the cause of this cooling remains an open question.

5. Conclusions

The annual growth rate of stalagmite XL21 from Xianglong Cave, on the south flank of the Qinling Mountains, central China, showed a significantly positive correlation with local temperature variability. Based on correlation analysis, the temperature of P_9-5 was quantitatively reconstructed. An increasing trend over the last 95 years, especially during the last 30 years, was observed in the reconstruction. Four notably colder periods occurred: in the early 1930s, the late 1950s, the early 1980s, and the early 1990s. Three notably warmer periods also occurred: from the late 1930s to the 1940s, the early 1970s, and from the late 1990s to the present. Temperature variability in central China is very similar to that in the Northern Hemisphere and global patterns. The cooling signal preserved in the stalagmite laminae from the 1980s to the early 1990s, which interrupted the warming trend that began in the 1960s, is

not evident in the mean temperature series from China, the Northern Hemisphere, neither the global record.

Acknowledgments

We thank Dr. Guoli Tang, Dr. Jiangfeng Shi and NOAA's National Climatic Data Center for providing the temperature datasets. We acknowledge Dr. D. Rudzka and the other two anonymous reviewers, as well as the editor (Prof. Xiaoping Yang) for their constructive comments and suggestions. This work was supported by the CAS Strategic Priority Research Program (grant XDA05080502); Key Program of the Chinese Academy of Sciences (grant KZZD-EW-04-01); National Science Foundation of China (grant 41001061); National Basic Research Program of China (grant 2013CB955902; 2010CB833405).

References

Baker, A., Asrat, A., Fairchild, I.J., Leng, M.J., Wynn, P.M., Bryant, C., Genty, D., Umer, M., 2007. Analysis of the climate signal contained within $\delta^{18}O$ and growth rate parameters in two Ethiopian stalagmites. Geochimica et Cosmochimica Acta 71, 2975–2988.

Baker, A., Bradley, C., 2010. Modern stalagmite $\delta^{18}O$: instrumental calibration and forward modelling. Global and Planetary Change 71, 201–206.

Baker, A., Genty, D., Dreybrodt, W., Barnes, W.L., Mockler, H.J., Grapes, J., 1998. Testing theoretically predicted stalagmite growth rate with recent annually laminated samples: implications for past stalagmite deposition. Geochimica et Cosmochimica Acta 62, 393–404.

Baker, A., Smith, C.L., Jex, C., Fairchild, I.J., Genty, D., Fuller, L., 2008. Annually laminated speleothems: a review. International Journal of Speleology 37, 193–206.

Baldini, J.U.L., 2010. Cave atmosphere controls on stalagmite growth rate and palaeoclimate records. In: Geological Society, London, Special Publications, vol. 336, pp. 283–294.

Bar-Matthews, M., Ayalon, A., Matthews, A., Sass, E., Halicz, L., 1996. Carbon and oxygen isotope study of the active water-carbonate system in a karstic Mediterranean cave: implications for paleoclimate research in semiarid regions. Geochimica et Cosmochimica Acta 60, 337–347.

Brook, G.A., Rafter, M.A., Railsback, L.B., Sheen, S.-W., Lundberg, J., 1999. A high-resolution proxy record of rainfall and ENSO since AD 1550 from layering in stalagmites from Anjohibe Cave, Madagascar. The Holocene 9, 695–705.

Burns, S.J., Fleitmann, D., Mudelsee, M., Neff, U., Matter, A., Mangini, A., 2002. A 780-year annually resolved record of Indian Ocean monsoon precipitation from a speleothem from south Oman. Journal of Geophysical Research 107, 4434–4442.

Cai, B., Zhu, J., Ban, F., Tan, M., 2011. Intra-annual variation of the calcite deposition rate of drip water in Shihua Cave, Beijing, China and its implications for palaeoclimatic reconstructions. Boreas 40, 525–535.

Chen, H., Sun, Z., Min, J., 1999. The relationships between Eurasian winter snow cover anomaly and EAWM, China winter air temperature. Journal of Nanjing Institute of Meteorology 22, 609–615 (in Chinese with English abstr.).

Chen, Z., Zhang, X., He, X., Davi, N.K., Cui, M., Peng, J., 2013. Extension of summer (June–August) temperature records for northern Inner Mongolia (1715–2008), China using tree rings. Quaternary International 283, 21–29.

Cheng, H., Edwards, R.L., Broecker, W.S., Denton, G.H., Kong, X., Wang, Y., Zhang, R., Wang, X., 2009. Ice age terminations. Science 326, 248–252.

Chu, G., Sun, Q., Wang, X., Liu, M., Lin, Y., Xie, M., Shang, W., Liu, J., 2012. Seasonal temperature variability during the past 1600 years recorded in historical documents and varved lake sediment profiles from northeastern China. The Holocene 22, 785–792.

Cook, E.R., 1990. Bootstrap confidence intervals for red spruce ring-width chronologies and an assessment of age-related bias in recent growth trends. Canadian Journal of Forest Research 20, 1326–1331.

Cook, E.R., Anchukaitis, K.J., Buckley, B.M., D'Arrigo, R.D., Jacoby, G.C., Wright, W.E., 2010. Asian monsoon failure and megadrought during the last millennium. Science 328, 486–489.

Cook, E.R., Meko, D.M., Stahle, D.W., Cleaveland, M.K., 1999. Drought reconstructions for the continental United States. Journal of Climate 12, 1145–1162.

Ding, Y., Ren, G., Shi, G., Gong, P., Zheng, X., Zhai, P., Zhang, D., Zhao, Z., Wang, S., Wang, H., Luo, Y., Chen, D., Gao, X., Dai, X., 2007. China's national assessment report on climate change (I): climate change in China and the future trend. Advances in Climate Change Research 3, 1–5.

Dreybrodt, W., 1980. Deposition of calcite from thin films of natural calcareous solutions and the growth of speleothem. Chemical Geology 29, 80–105.

Dreybrodt, W., 1981. The kinetics of calcite precipitation from thin films of calcareous solutions and the growth of speleothems: revisited. Chemical Geology 32, 237–245.

Duan, W., Cai, B., Tan, M., Liu, H., Zhang, Y., 2012. The growth mechanism of the aragonitic stalagmite laminae from Yunnan Xianren Cave, SW China revealed by cave monitoring. Boreas 41, 113–123.

Edwards, R.L., Chen, J.H., Wasserburg, G.J., 1987. ^{238}U-^{234}U-^{230}Th-^{232}Th systematic and the precise measurement of time over the past 500,000 years. Earth and Planetary Science Letters 81, 175–192.

Fairchild, I.J., Smith, C.L., Baker, A., Fuller, L., Spotl, C., Mattey, D., McDermott, F., E.I.M.F., 2006. Modification and preservation of environmental signals in speleothems. Earth-Science Reviews 75, 105–153.

Frisia, S., Borsato, A., Preto, N., McDermott, F., 2003. Late Holocene annual growth in three Alpine stalagmites records the influence of solar activity and the North Atlantic. Earth and Planetary Science Letters 216, 411–424.

Ge, Q., Zheng, J., Fang, X., Man, Z., Zhang, X., Zhang, P., Wang, W.-C., 2003. Winter half-year temperature reconstruction for the middle and lower reaches of the Yellow River and Yangtze River, China, during the past 2000 years. The Holocene 13, 933–940.

Ge, Q., Zheng, J., Hao, Z., Shao, X., Wang, W.-C., Luterbacher, J., 2010. Temperature variation through 2000 years in China: an uncertainty analysis of reconstruction and regional difference. Geophysical Research Letters 37, L03703.

Genty, D., Baker, A., Vokal, B., 2001. Intra- and inter-annual growth rate of modern stalagmites. Chemical Geology 176, 191–212.

Gong, D., Wang, S., Zhu, J., 2001. East Asian winter monsoon and Arctic oscillation. Geophysical Research Letters 28, 2073–2076.

Gou, X., Peng, J., Chen, F., Yang, M., Levia, D.F., Li, J., 2008. A dendrochronological analysis of maximum summer half-year temperature variations over the past 700 years on the northeastern Tibetan Plateau. Theoretical and Applied Climatology 93, 195–206.

Hao, Z.X., Zheng, J.Y., Ge, Q.S., Wang, W.C., 2012. Winter temperature variations over the middle and lower reaches of the Yangtze River since 1736 AD. Climate of the Past 8, 1023–1030.

IPCC, 2007. Climate Change 2007: the Physical Science Basis. Cambridge University Press, Cambridge.

Jaffey, A.H.K., Flynn, F., Glendenin, L.E., Bentley, W.C., Essling, A.M., 1971. Precision measurement of half-lives and specific activities of ^{235}U and ^{238}U. Physics Reviews C 4, 1889–1906.

Kalvová, J., Nemesová, I., 1998. Estimating autocorrelations of daily extreme temperatures in observed and simulated climates. Theoretical and Applied Climatology 59, 151–164.

Lawrimore, J.H., Menne, M.J., Gleason, B.E., Williams, C.N., Wuertz, D.B., Vose, R.S., Rennie, J., 2011. An overview of the global historical climatology network monthly mean temperature data set, version 3. Journal of Geophysical Research 116, D19121. http://dx.doi.org/10.1029/2011JD016187.

Li, Z.-S., Zhang, Q.-B., Ma, K., 2012. Tree-ring reconstruction of summer temperature for A.D. 1475-2003 in the central Hengduan Mountains, Northwestern Yunnan, China. Climatic Change 110, 455–467.

Linderholm, H.W., Chen, D., 2005. Central Scandinavian winter precipitation variability during the past five centuries reconstructed from *Pinus syvestris* tree rings. Boreas 34, 43–52.

Liu, X., Fang, J., Yang, X., Li, X., 2003. Climatology of dekadly precipitation around the Qinling mountains and characteristics of its atmospheric circulation. Arid Meteorology 21, 8–13 (in Chinese with English abstr.).

Liu, X., Qin, D., Shao, X., Chen, T., Ren, J., 2005. Temperature variations recovered from tree-rings in the middle Qilian Mountain over the last millennium. Science in China Series D: Earth Sciences 48, 521–529.

Liu, Y., An, Z., Linderholm, H.W., Chen, D., Song, H., Cai, Q., Sun, J., Li, Q., Tian, H., 2009a. Annual temperatures during the last 2485 years in the Eastern Tibetan Plateau inferred from tree rings. Science in China Series D: Earth Sciences 52, 348–359.

Liu, Y., Linderholm, H.W., Song, H., Cai, Q., Tian, Q., Sun, J., Chen, D., Simelton, E., Seftigen, K., Tian, H., Wang, R., Bao, G., An, Z., 2009b. Temperature variations recorded in *Pinus tabulaeformis* tree rings from the southern and northern slopes of the central Qinling Mountains, central China. Boreas 38, 285–291.

Mariethoz, G., Kelly, B.F.J., Baker, A., 2012. Quantifying the value of laminated stalagmites for paleoclimate reconstructions. Geophysical Research Letters 39, L05407.

Mattey, D., Lowry, D., Duffet, J., Fisher, R., Hodge, E., Frisia, S., 2008. A 53-year seasonally resolved oxygen and carbon isotope record from a modern Gibraltar speleothem: reconstructed drip water and relationship to local precipitation. Earth and Planetary Science Letters 269, 80–95.

McCabe, G.J., Markstrom, S.L., 2007. A Monthly Water-balance Driven by a Graphical User Interface. US Geological Survey Open-File Report 2007-1088, p. 6.

McDermott, F., 2004. Palaeo-climate reconstruction from stable isotope variations in speleothems: a review. Quaternary Science Reviews 23, 901–918.

Meko, D.M., Graybill, D.A., 1995. Tree-ring reconstruction of upper Gila River discharge. Journal of the American Water Resource Association 31, 605–616.

Polyak, V.J., Asmerom, Y., 2001. Late Holocene climate and cultural changes in the southwestern United States. Science 294, 148–151.

Proctor, C.J., Baker, A., Barnes, W.L., Gilmour, M.A., 2000. A thousand year speleothem proxy record of North Atlantic climate from Scotland. Climate Dynamics 16, 815–820.

Ruan, J., Hu, C., 2010. Seasonal variations and environmental controls on stalagmite calcite crystal growth in Heshang Cave, central China. Chinese Science Bulletin 55, 1–7.

Shao, X., 2012. A preliminary reconstruction of temperature in the eastern Qaidam Basin, northeaster Tibetan Plateau, China. Quaternary International 279-280, 444.

Shen, C.-C., Cheng, H., Edwards, R.L., Moran, S.B., Edmonds, H.N., Hoff, J.A., Thomas, R.B., 2003. Measurement of attogram quantities of ^{231}Pa in dissolved and particulate fractions of seawater by isotope dilution thermal ionization mass spectroscopy. Analytical Chemistry 75, 1075–1079.

Shen, C.-C., Wu, C.-C., Cheng, H., Edwards, R.L., Hsieh, Y.-T., Gallet, S., Chang, C.-C., Li, T.-Y., Lam, D.D., Kano, A., Hori, M., Spötl, C., 2012. High-precision and high-resolution carbonate ^{230}Th dating by MC-ICP-MS with SEM protocols. Geochimica et Cosmochimica Acta 99, 71–86.

Shi, J., Lu, H., Wan, J., Li, S., Hongshan, N., 2009. Winter-half year temperature reconstruction of the last century using *Pinus Armandii* Franch tree-ring width chronology in the Eastern Qinling Mountains. Quaternary Sciences 29, 831–836 (in Chinese with English abstr.).

Spötl, C., Fairchild, I.J., Tooth, A.F., 2005. Cave air control on dripwater geochemistry, Obir Caves (Austria): implications for speleothem deposition in dynamically. Geochimica et Cosmochimica Acta 69, 2451–2468.

Tan, L., Cai, Y., An, Z., Yi, L., Zhang, H., Qin, S., 2011. Climate patterns in north central China during the last 1800 yr and their possible driving force. Climate of the Past 7, 685–692.

Tan, L., Cai, Y., Cheng, H., An, Z., Edwards, R.L., 2009. Summer monsoon precipitation variations in central China over the past 750 years derived from a high-resolution absolute-dated stalagmite. Palaeogeography, Palaeoclimatology, Palaeoecology 280, 432–439.

Tan, M., Baker, A., Genty, D., Smith, C., Esper, J., Cai, B., 2006. Applications of stalagmite laminae to paleoclimate reconstructions: comparison with dendrochronology/climatology. Quaternary Science Reviews 25, 2103–2117.

Tan, M., Liu, T., Hou, J., Qin, X., Zhang, H., Li, T., 2003. Cyclic rapid warming on centennial-scale revealed by a 2650-year stalagmite record of warm season temperature. Geophysical Research Letters 30, 191–194.

Tang, G., Ding, Y., Wang, S., Ren, G., Liu, H., Zhang, L., 2010. Comparative analysis of the time series of surface air temperature over China for the last 100 years. Advances in Climate Change Research 1, 11–19.

Taylor, S.R., McLennan, S.M., 1995. The geochemical evolution of the continental crust. Reviews of Geophysics 33, 241–265.

Thompson, L.G., Yao, T., Davis, M.E., Mosley-Thompson, E., Lin, P., Mashiotta, T.A., Mikhalenko, V.N., Zagordonov, V.S., 2006. Holocene climate variability archived in the Puruogangri ice cap on the central Tibetan Plateau. Annals of Glaciology 43, 61–69.

Thornthwaite, C.W., 1948. An approach toward a rational classification of climate. Geographical Review 38, 55–94.

Vaks, A., Bar-Matthews, M., Ayalon, A., Schilman, B., Gilmour, M., Hawkesworth, C.J., Frumkin, A., Kaufman, A., Matthews, A., 2003. Paleoclimate reconstruction based on the timing of speleothem growth and oxygen and carbon isotope composition in a cave located in the rain shadow in Israel. Quaternary Research 59, 182–193.

Wang, N., Yao, T., Pu, J., Zhang, Y., Sun, W., 2006. Climatic and environmental changes over the last millennium recorded in the Malan ice core from the northern Tibetan Plateau. Science in China Series D: Earth Sciences 49, 1079–1089.

Wang, N., Yao, T., Pu, J., Zhang, Y., Sun, W., Wang, Y., 2003. Variations in air temperature during the last 100 years revealed by δ^{18}O in the Malan ice core from the Tibetan Plateau. Chinese Science Bulletin 48, 2134–2138.

Xiao, S., Liu, W., Li, A., Yang, S., Lai, Z., 2010. Pervasive autocorrelation of the chemical index of alteration in sedimentary profiles and its palaeoenvironmental implications. Sedimentology 57, 670–676.

Yang, B., Bräuning, A., Liu, J., Davis, M.E., Yajun, S., 2009. Temperature changes on the Tibetan Plateau during the past 600 years inferred from ice cores and tree rings. Global and Planetary Change 69, 71–78.

Yang, Y., 2007. The preliminary study in reconstructing the mean winter temperature in Kunming during 1721-1900 AD. Journal of Chinese Historical Geography 22, 17–31 (in Chinese).

Yao, T., Guo, X., Thompson, L., Duan, K., Wang, N., Pu, J., Xu, B., Yang, X., Sun, W., 2006. δ^{18}O record and temperature change over the past 100 years in ice cores on the Tibetan Plateau. Science in China Series D: Earth Sciences 49, 1–9.

Yao, T., Shi, Y., Thompson, L.G., 1997. High resolution record of paleoclimate since the Little Ice Age from the Tibetan ice cores. Quaternary International 37, 19–23.

Yi, L., Yu, H., Ge, J., Lai, Z., Xu, X., Qin, L., Peng, S., 2012. Reconstructions of annual summer precipitation and temperature in north-central China since 1470 AD based on drought/flood index and tree-ring records. Climatic Change 110, 469–498.

Zhang, T., Yuan, Y., Wei, W., Yu, S., Zhang, R., Shang, H., Chen, F., Fan, Z., Qin, L., 2013. Tree-ring-based temperature reconstruction for the northern Greater Higgnan Mountains, China, since A.D. 1717. International Journal of Climatology 33, 422–429.

Zhao, J., 1995. Chinese Physical Geography. Higher Education Press, Beijing (in Chinese).

Zhu, Y., 2008. An index of East Asian winter monsoon applied to description the Chinese mainland winter temperature changes. Acta Meteorologica Sinica 22, 522–529 (in Chinese with English abstr.).